PROCEEDINGS OF SCIENCE

Model of a Cryogenic Detector for Fast Neutron Spectroscopy Using a Silicon Absorber

Stephen J Smith
University of Leicester, Department of Physics and Astronomy
Space Research Centre, University Rd, Leicester, LE1 7RH, UK.
E-mail: sjs@star.le.ac.uk

John I W Watterson
University of the Witwatersrand, School of Physics,
Private Bag 3, PO WITS, Johannesburg, 2050, South Africa
E-mail: wattersonj@physics.wits.ac.za

Richard M Ambrosi*
University of Leicester, Department of Physics and Astronomy
Space Research Centre, University Rd, Leicester, LE1 7RH, UK.
E-mail: rma@star.le.ac.uk

Microcalorimeters such as Transition Edge Sensors (TESs) are promising devices that can be used for photon and particle detection over a wide energy range. The theoretical energy resolution of a few eV in the soft X-ray band make such devices an exciting prospect for future observatories in the space sciences. The idea of using a similar technique for fast neutron spectroscopy has been explored using boron or lithium-based absorbers and an experimental energy resolution of less than 1% was obtained. The aim of this work is to investigate the extension of this capability to fast neutrons above 5 MeV using TES-based spectrometers and to develop the new idea of energy discrimination based on threshold reactions in the absorber. In this paper we explore the development of an instrument for fast neutron spectroscopy with optimum spectral resolution for both terrestrial and space-based applications. We investigate a position-sensitive microcalorimeter read-out system at both ends of a silicon absorber. We use Monte Carlo methods to investigate neutron interactions with the silicon absorber and develop a response function for such a detector.

International Workshop on Fast Neutron Detectors
University of Cape Town, South Africa
April 3 – 6, 2006

* Speaker

© Copyright owned by the author(s) under the terms of the Creative Commons Attribution-NonCommercial-ShareAlike Licence.

PoS(FNDA2006)012

1. Introduction

The detection of neutrons has a number of different applications in space science as well as in many other fields. In space science there are two main interests. One interest is in the detection of the secondary neutrons produced by nuclear reactions with protons in the solar wind in planetary exploration. The neutrons detected in planetary orbit can be an indicator of the presence of hydrogen, and therefore possibly water, on planetary surfaces. The other is in the neutron component of the radiation background in satellites and space probes, which affects the radiation fluence interacting with detectors and electronics in the satellite.

In non-destructive testing (NDT), fast neutron radiography offers particular advantages such as: penetrability through high-density materials and the technique of element-sensitive imaging through fast neutron resonance radiography (FNRR) has recently been developed [1-4].

Fast neutron resonance radiography has been proposed as a tool for the detection of explosives, contraband and for the screening of cargo; it is being implemented in mining to search for minerals of specific composition and for nuclear stockpile stewardship as part of non-proliferation treaties. In this paper, we describe a high-resolution spectroscopic detector for fast neutron imaging. In this paper we focus on 8 MeV neutrons as part of a continuing study to explore the use of the resonance in the cross section spectrum of carbon in order to find carbon rich inclusions in mineral samples. This study is based on a position-sensitive microcalorimeter, under development at the University of Leicester for high-resolution X-ray spectroscopy. The proposed detector would eliminate the background from scattered, low energy neutrons in many applications of FNRR. It would have applications in planetary science, in the detection of contraband substances such as drugs and explosives as well as illicit fissile materials and neutron sources, and also as a tool for calibrating neutron sources [5]. In general fast neutron spectroscopy poses many problems that have not yet been solved. Many current fast neutron spectrometers are based on gas detectors or on liquid scintillators with pulse shape discrimination. The energy discrimination of these methods is poor and the presence of a gamma-ray background is a major source of interference. The most accurate way of doing neutron spectroscopy relies on time of flight techniques with a pulsed accelerator but this technique is restricted in its application as it can only be used with nanosecond neutron pulses [6].

2 Detection of Neutrons

Because neutrons produce no direct ionisation, detectors must be based on the ionising properties of secondary particles from nuclear reactions for example (n,n), (n,p), (n,α) and (n,γ). The reaction $^{10}B(n,\alpha)^{7}Li$ is commonly used for the detection of thermal neutrons. If the material of the detector absorbs the energy of the ions and other secondary particles produced, then, the total energy deposited is equivalent to the Q-value of the reaction plus the energy of the neutron.

PoS(FNDA2006)012

In this paper we concentrate on the possibility of using silicon as the absorber in a detector for fast neutrons. Silicon has a number of advantages in this application for the detection of neutrons with energies above about 5 MeV. At these energies the neutrons are above the thresholds for the (n,p), (n,α) and (n,d) reactions in silicon. The charged particles produced in these reactions have high linear energy transfers (LETs) and lose their energy close to the interaction point. This energy is equal to the Q-value of the reaction plus the kinetic energy of the neutron and provided that this energy can be detected neutron spectroscopy is possible. The combination of a silicon absorber with a microcalorimeter, such as a TES, offers the prospect of such a detector.

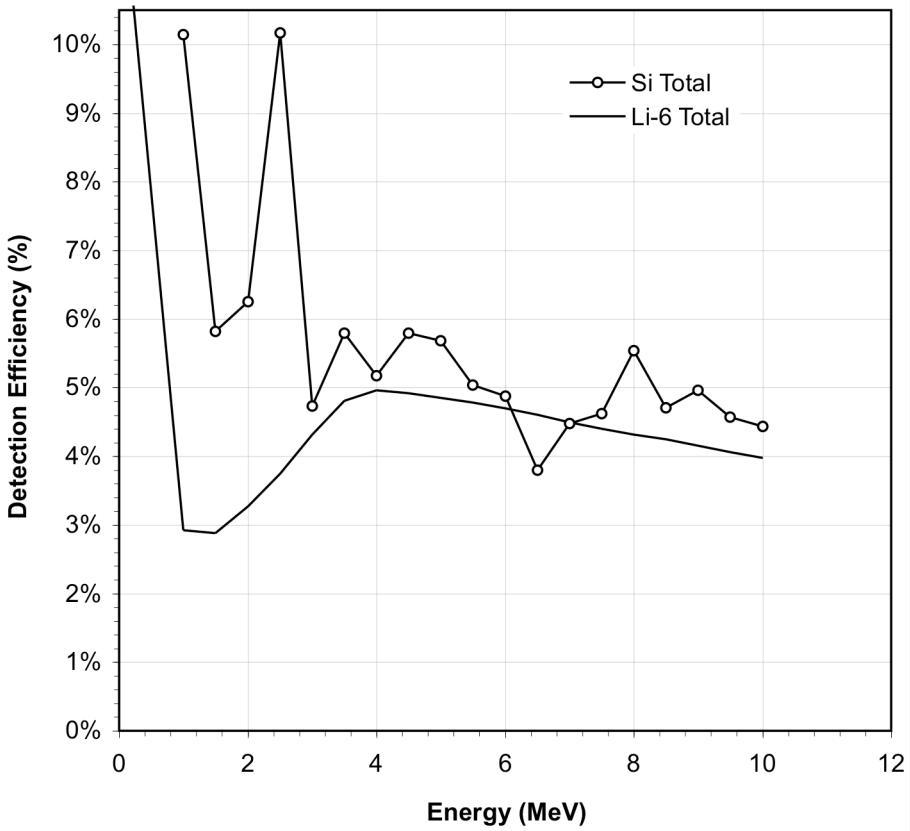

Figure 1. Detection efficiency of Si and ^{6}Li as a function of neutron energy assuming a 100% concentration of ^{6}Li in the absorber. The total cross section was used in the evaluation of the efficiency values. In both cases the absorber was 5 mm thick.

A particular advantage of a detector of this type utilising threshold reactions (approximately 5 MeV for these reactions) is that neutron scattering events can be discriminated from neutrons in the primary beam. Another commonly used neutron detecting element, ^{6}Li is a naturally occurring stable isotope of Li with an isotopic fraction of 7.6% compared to ^{7}Li, which is the dominant isotope. The absorber would have to be significantly enriched with ^{6}Li in order to achieve a detection efficiency comparable to Si if the (n,p) and (n,t) reactions in Li were to be exploited. Figure 1 shows the detection efficiency of naturally occurring Si and ^{6}Li, calculated

PoS(FNDA2006)012

using the total neutron cross sections for the materials, as a function of neutron energy assuming a 100% concentration of ^{6}Li. Figure 2 shows the same plot for the capture cross sections, indicating that the efficiency of Li as an absorber would be significantly worse than Si at 8 MeV. In both cases the thicknesses of the absorbers was 5 mm. The capture reactions, which produce secondary particles in the form of (n,p), (n,α), (n,d) reactions, are of primary interest since these will lose all their energy in the absorber with distinct energy signatures.

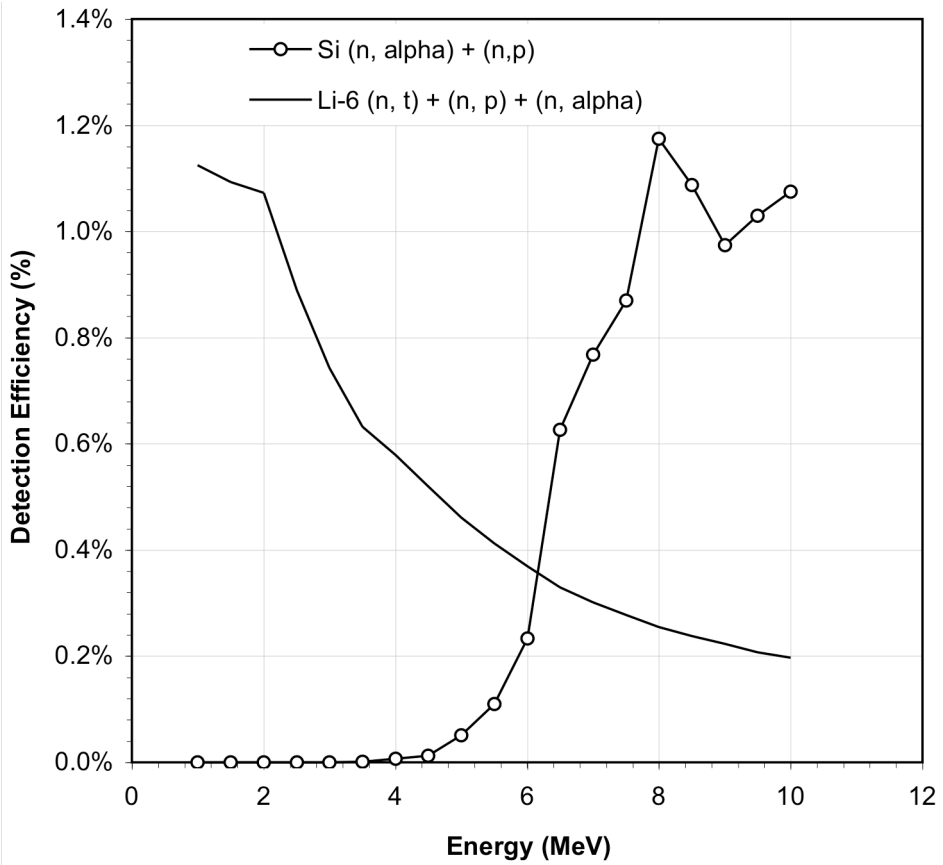

Figure 2. Detection efficiency of Si and ^{6}Li as a function of neutron energy for various capture reactions only. Once again a 100% ^{6}Li concentration is assumed. In both cases the absorber was 5mm thick.

3 Cryogenic Detectors

Microcalorimeters such as Transition Edge Sensors (TESs) [8] or Metallic Magnetic Calorimeters (MMCs) [9], are promising devices that can be used for photon and particle detection over a wide energy range. These microcalorimeters have theoretical ~eV energy resolution in the soft X-ray energy band (0.1 to 10 keV), making such devices an exciting prospect for future X-ray astronomy observatories such as the X-ray Evolving Universe Spectrometer (XEUS) [10], currently under study by the European Space Agency.

PoS(FNDA2006)012

The capability of using cryogenic detectors for particle detection has been explored in the past. For example, De Marcillac et al. [11] describe a bolometer based on a thermistor with 6LiF absorber for the detection of 5 MeV α-particles and 5 MeV neutron capture events in both cases demonstrating a resolution of ~16 keV (FWHM). Similarly, Silver et al. [12] have described the use of 6LiF absorbers for bolometeric neutron detection with a FWHM resolution of 39 keV for 5.3 MeV α-particles and 170 keV for 4 MeV alpha particles from thermal neutrons. In both these examples the authors make use of the ^{6}Li(n,α) capture reaction, which has a Q-value of + 4.78 MeV and the absorption cross-section is 0.095 b at 4 MeV. Because of the positive Q value, this reaction is very sensitive to thermal and low energy neutrons, in contrast to the silicon reactions investigated here.

Frank et al. [13] used a 4 × 2 × 1 cm^3 Si absorber with an iridium TES for particle detection and demonstrated a 60 keV energy resolution associated with 5 MeV α-particles. Niedermayr et al. [14] investigated the use of boron or lithium-based absorbers, which have large cross sections for thermal and epithermal neutrons. Their aim was a 0.1% energy resolution for 1-21 MeV neutrons and at least a 1% efficiency. In a first test detector Niedermayr et al. used a 1 mm^3 TiB_2 absorber with a Mo/Cu TES bi-layer and demonstrated a resolution of 5.5 keV FWHM for the 2.792 MeV α-particle group produced by thermal neutrons. Our aim is to extend this capability to fast neutrons above 5 MeV with a detection efficiency of ≥1%.

Large absorber, position-sensitive cryogenic detectors [15] offer an alternative approach to the more common pixellated arrays. Such devices operate by the principle of heat diffusion whereby two or more sensors occupy a single large absorber. The sum of the signals gives the total energy of the event and the interaction position is given by the difference in signals. Such detectors offer a comparative energy and spatial resolution relative to their pixellated counterparts but with a reduced number of readout channels. At the University of Leicester, we are developing Distributed Read-Out Imaging Devices (DROIDs) as alternative focal plane detectors for future X-ray astronomy missions such as XEUS. Our prototype DROIDs consist iridium TESs either side of a linear 5 mm long X-ray absorber. Further details on these devices are reported elsewhere [16-18]. Such devices can, potentially, be redesigned and used as particle detectors, specifically for fast neutron spectroscopy in the 5-21 MeV range.

We have established a finite-element model (FEM) to estimate the energy and spatial resolutions across the DROID detectors – the full details of which are incorporated in a separate study [19]. The model, based on the assumption that the energy transport is diffuse (see Section 6), is used to numerically calculate the energy and position resolution of the devices. Using the signal processing algorithms and FEM developed in [19], we calculate, assuming a typical TES DROID with a 10 cm long Si absorber and 5 × 5 mm^2 cross sectional area, a FWHM energy resolution of < 0.01 % in the range 5-21 MeV, with corresponding spatial resolutions of the order 10s of microns. The intrinsic detector resolution will not however limit its performance;

PoS(FNDA2006)012

the resolution limit will be determined by the response (thermalisation effects) of the Si absorber to detected neutron events. The 100 μs time constant associated with TES based detectors and the lengthy signal processing time required [16-19] for such detectors (as much as 100 times the time constant) implies that the time resolution of these detectors is of the order of 10 ms. This implies that the detector would lend itself to neutron counting applications, where fluxes are low, or that the flux would have to be reduced in order for the detector to cope. Thus we must consider the detection process in Si and investigate the response function of the detector.

4 Modelling Neutron Interactions in Silicon using MCNP

Monte Carlo programmes, such as the Monte Carlo N-Particle transport code (MCNPX^{TM}) [20], provide a way of modelling the complicated interactions between neutrons and matter. These interactions are directly relevant to the detection of neutrons. In this work we have used MCNP to assist in the evaluation of silicon as a fast neutron detector.

In the problem under study, our interest is in tracking the neutron energy deposition process, either through scattering, capture or γ-ray emission and of determining over what detector volume the energy from a detected neutron is deposited. This will enable us to work out a response function for the detector and determine its potential for fast neutron spectroscopy.

We are interested both in the fall-off of the deposited energy with distance from the neutron trajectory and also in the way in which the energy is deposited. We would like to know how much energy is deposited in the different modes: in the recoil of the Si nuclei (inducing lattice vibrations or generating phonons) and in the protons, α-particles, electrons and photons produced by the interactions. It is important to determine how the energy is deposited around a neutron track that penetrates an absorber as this provides a measure of the spatial resolution limits that will be imposed on the detector. Of particular interest in this application are the (n,p) and (n,α) reactions in Si.

Figure 3 shows the predictions of MCNPX for the total energy absorbed in the silicon wafer as a function of the incident neutron energy and a comparison of these predictions with the excitation functions for various reactions producing charged particles. There is a sharp rise in the energy deposited as the threshold for the $^{28}Si(n,p)^{28}Al$ and $^{28}Si(n,\alpha)^{25}Mg$ reactions is exceeded. The deposited energy rises from 0.01 MeV/g per incident neutron at 2 MeV to about 0.35 MeV/g per incident neutron at 8 MeV, showing a behaviour very similar to the sum of the cross-sections of these two reactions. It continues to rise but more slowly, even as these cross-sections decrease. This is because the cross-sections for the emission of multiple charged particles grow. This prediction by MCNPX demonstrates how such a detector would be relatively insensitive to neutrons with energies below about 5 MeV. The relatively small but

PoS(FNDA2006)012

nevertheless finite value of the energy deposited even at 2 MeV (incident neutron energy) is thought to result from the recoil of the silicon nuclei produced by the elastic scattering of the neutrons. This point is discussed further below.

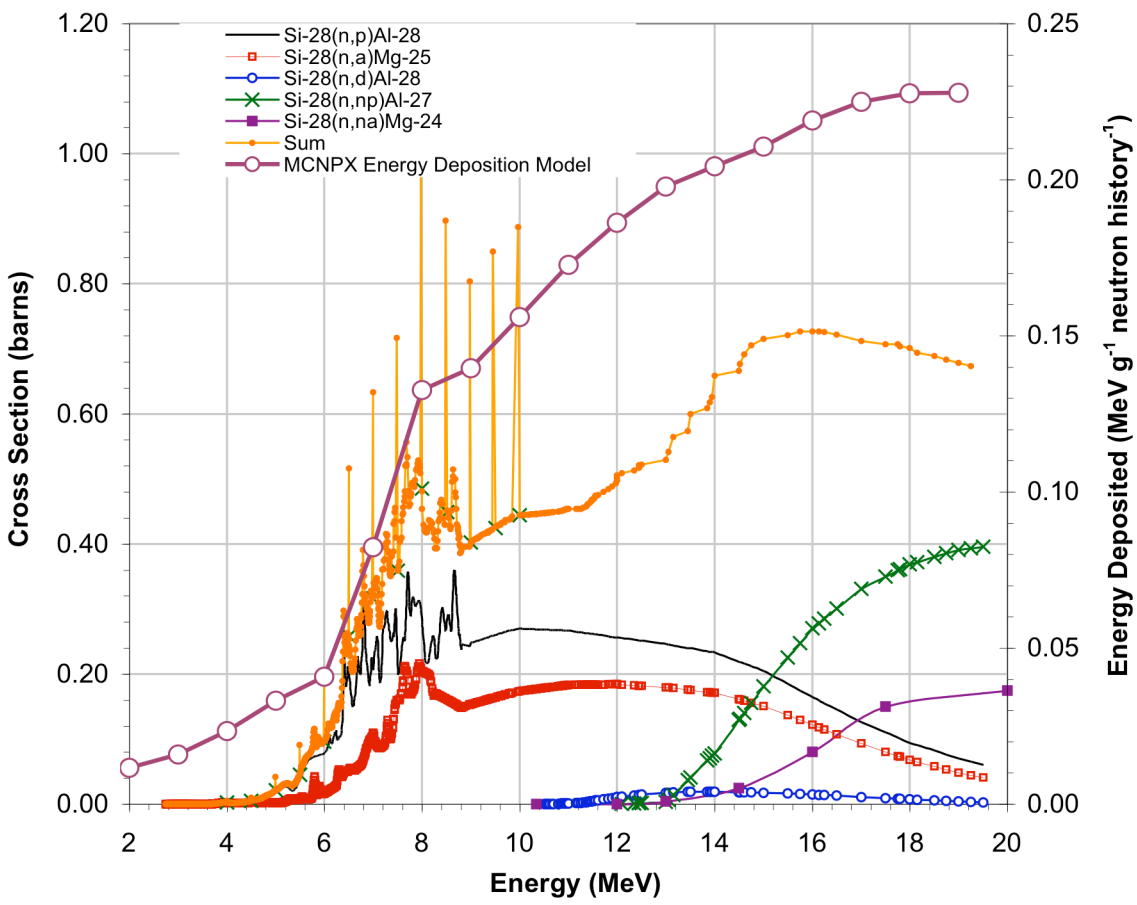

Figure 3. Energy deposited in the silicon wafer as a function of the incident neutron energy compared with the excitation functions for five charged-particle producing reactions and their sum. The axis on the right refers to the MCNPX modelled energy deposition in a Si absorber.

At an incident neutron energy of 8 MeV the energy dissipated within the silicon has risen sharply. MCNPX has been used to examine in detail how the energy is absorbed and the spatial distribution of this absorption at this neutron energy. In previous studies by Ambrosi and Watterson [1,3] 8 MeV accelerator-based neutron sources have been used in resonance neutron radiography experiments and this energy is also of particular interest in FNRR.

Using MCNPX we calculate the energy deposition as a function of distance from the incident neutron track. Figure 4 shows the total energy deposited by an 8 MeV neutron in Si (averaged over 10^6 events) as a function of the distance using this tally with a resolution of 10 micrometers. Along the track (within a couple of microns, say), ~ 70% of the energy deposited

PoS(FNDA2006)012

is from the direct recoil of the silicon nuclei. This energy is deposited over a very short range and drops off rapidly with distance. At a distance of 10 μm almost all of the energy deposited is from the alpha particles from the reaction $^{28}Si(n,\alpha)^{25}Mg$. There is a rapid fall-off with distance and over 80% of the energy is deposited within about 30 μm of the trajectory. At distances greater than 30 μm the deposited energy is from the protons and this component falls off slowly with distance. The range of the protons is significantly greater than 100 μm.

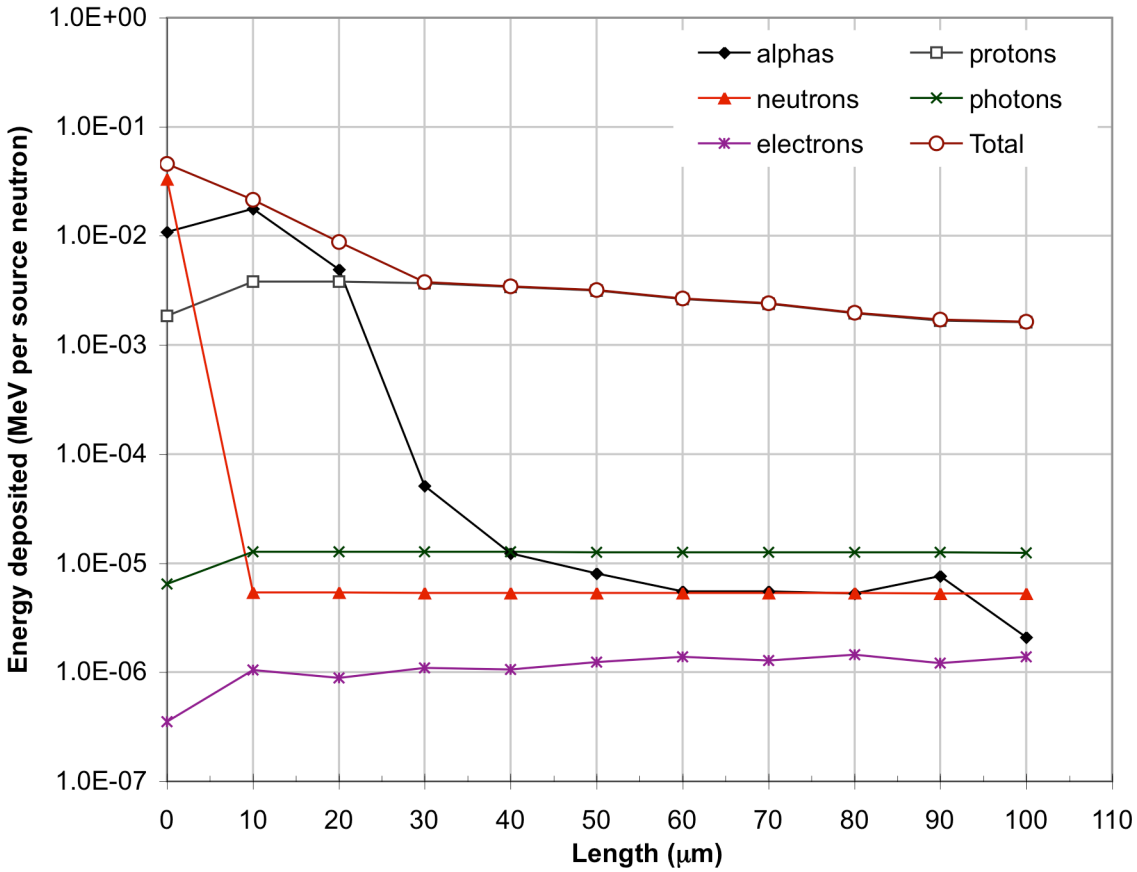

Figure 4. Shows average energy deposition as a function of distance from the neutron trajectory for 10^6 events. Also shown is the deposition due to each individual species. The data is derived using MCNPX with an incident neutron energy of 8 MeV.

The neutrons thus deposit most of their energy along the track, through the recoil of the Si nuclei. By far the major contributors to the energy deposition at a distance of ~ 10 μm (at this neutron energy) are α-particles which show an increasing dE/dx up to ~ 10 μm before rapidly dropping off. The contribution to energy deposition from γ-rays and from electrons is very low. The figure for the γ-rays is about one thousandth of the total and that for the electrons is about one ten-thousandth of the total at a distance of 20 μm. At larger distances the relative contributions increase and by 100 μm they have risen by an order of magnitude. These data

PoS(FNDA2006)012

indicate that energy deposition does occur over comparatively short length scales implying that a degree of spatial resolution of the order 100 μm should be achievable.

5 Neutron Spectroscopy

In order to assess what sort of energy resolution could be achieved with a microcalorimeter based detector it is necessary to establish the response function. Because the cross-sections are a function of energy, the detector response function will also be different according to the energy of the source neutron and therefore must be evaluated over the energy range of interest.

If all the energy of any interacting neutron is transferred to the medium i.e. to lattice vibrations the first requirement for a detector with a good intrinsic resolution has been met. In neutron (and γ-ray) interactions, this does not happen because scattered neutrons and high-energy γ-rays can escape from the detector volume.

A large number of the interactions are neutron recoil. These leave different amounts of energy in the detector depending on the scattering angle. If we assume that the scattering is isotropic in the centre of mass system then the number of particles scattered through angles between θ and θ+dθ will be proportional to the solid angle $d\Omega = 2\pi \sin\theta\, d\theta$. From elementary conservation of energy and momentum we know that the energy of neutrons scattered E_{scatt} through an angle θ (in the centre of mass system) by a nucleus of mass A is given by [21]:

$$E_{scatt} = E_0\left[\frac{1 + A^2 + 2A\cos\theta}{(1+A)^2}\right], \tag{1}$$

where E_0 is the initial energy. The amount of energy deposited in the recoil is then:

$$E_{dep} = E_0 - E_{scatt} = E_0\left[1 - \frac{1 + A^2 + 2A\cos\theta}{(1+A)^2}\right] = 2AE_0\left[\frac{1-\cos\theta}{(1+A)^2}\right], \tag{2}$$

differentiating to obtain the relationship between the change in energy and the angle, we obtain:

$$\sin\theta d\theta = \left[\frac{(1+A)^2}{2AE_0}\right] dE_{dep} \tag{3}$$

Thus in the response function, the number of events in each energy bin, dE_{dep}, will be a constant over the energy region from zero to the maximum energy deposited E_{max}. For direct neutron interactions with any material the maximum energy lost to the medium will occur for

PoS(FNDA2006)012

head on collisions where the neutron scattering angle is θ = 180°. From Equation 2, the maximum energy deposited is:

$$E_{\max} = E_0\left[1-\left(\frac{A-1}{A+1}\right)^2\right], \quad (4)$$

which for Si is $0.13E_0$. This determines the position of the edge from elastic scattering in the response function. The area of this, approximately rectangular, response function from the elastic scattering is proportional to the cross-section. In the case of inelastic scattering of the neutrons leaving the residual nucleus in an excited state, the positions of the edges are reduced proportionately. These edges will add. Consequently, the neutron recoil contribution in the response function will not be a 'boxcar' response but will be weighted toward the low energy end of the distribution. In the case of a Li absorber E_{max} is $0.49E_0$ and the neutrons will lose more energy with each interactions, as a result the energy distribution of the recoil continuum will extend to higher energies and be more intense in comparison to that for silicon.

The charged particles from the various reactions: (n,p), (n,α) and (n,d), for example, will deposit energy depending upon the Q-values of the reactions. Table 1 shows the Q-values for Si and for comparison we also show those for Li, which is also used in neutron detectors. Non-elastic scattering would be responsible for producing multiple proton and alpha particle signatures each at a specific energy depending on the energy of the associated gamma ray.

Table 1. Q-values.

	(n,p)	(n,α)	(n,d)
^{28}Si Q-value (MeV)	-3.860	-2.641	-9.360
^{28}Si Threshold (MeV)	3.999	2.749	9.698
^{6}Li Q-value (MeV)	2.725	4.783	-
^{6}Li Threshold (MeV)	3.182	0	-

The response function of the detector should take into account the contribution by gamma rays produced as a result of the inelastic and non-elastic scattering processes, since these gammas will have energies exceeding 1 MeV and given the size of the absorber in question, they will deposit little energy in the system. MCNPX results shown in Figure 4, predict that the total energy deposited by these events will be approximately three orders of magnitude less than that deposited by the charged particles. The energy deposited in individual events, by Compton scattering within the microcalorimeter volume, will be very small indeed. Depending on the resolving time and the neutron flux, multiple gamma ray events may contribute a constant background.

PoS(FNDA2006)012

In order to model the response function, the Monte Carlo code MCNP-X was used to determine how much energy would be deposited by the gamma rays associated with inelastic and non-elastic scattering events generated by 8 MeV neutrons interacting with a Si absorber. Table 2 lists some of the gamma ray energies associated with the first 5 excited states of the ^{29}Si compound nucleus.

Table 2. ^{28}Si adopted levels [7].

Eγ (MeV)	E_{level} (MeV)
1.779	1.779
2.839	4.618
3.201	4.980
4.497	6.276

The relative intensities of the events associated with the Si recoil interactions, (n,p), (n,a), and gamma rays produced can be calculated from the cross sections for the various reactions in relation to the total cross section for 8 MeV neutrons in silicon. In the model and intrinsic detector resolution 10 keV was selected to distinguish between the different components of the response and also given that most results in the literature quote resolution values that are tens of keV. Figure 5 shows the three components of the ideal modelled response function. The recoil distribution (left) indicating the weighting towards the low energy part of the spectrum and how the positions of the edges are reduced proportionately as the neutron energy decreases due to inelastic scattering. The positions of the expected means of the peaks associated with the proton, alpha events are shown in the middle panel in Figure 5; the primary alpha and proton events are at 5.36 MeV and 4.14. MeV respectively, while all the events associated with non-elastic scattering interactions are at lower energies. The small contribution from gamma rays is shown in the last panel on the right. The length of the absorber, 10 cm, implies that gammas travelling along the length of the absorber will deposit the most amount of energy, but the small fraction of these gamma rays implies that the gamma ray background should be low as most gammas will exit the absorber without interacting. The theoretical spectroscopic efficiency of this detector should not be limited by the intrinsic resolution of the detector nor the energy loss to gamma rays, the energy resolution of the detector will ultimately be limited, depending on the count rate at the detector, by the energy distribution of neutrons produced by the source [6].

PoS(FNDA2006)012

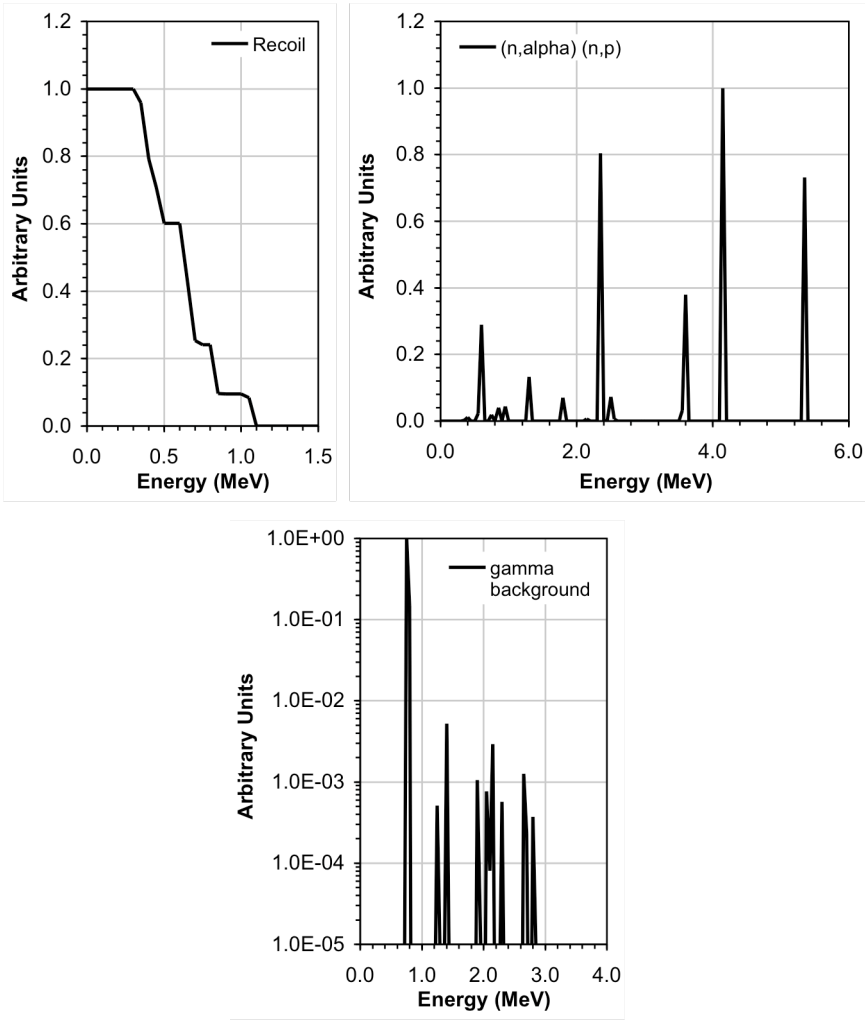

Figure 5. The ideal modelled response function. Each of the components of the response are separated out and displayed on a scale of 0 to 1. (top left) The elastic scattering Si recoil distribution is shown. (top right) The alpha particle and proton peaks (5.4 MeV and 4.1 MeV respectively) associated with the primary 8 MeV neutrons as well as all products of non-elastic scattering are shown. (bottom) The right the gamma ray background is shown.

Figure 6 shows the combined response function with all the weighting factors extracted from the cross sections of the different reactions taken into account. In the case of the gamma rays an additional weighting factor was introduced from the MCNPX™ modelling, which was used to determine the fraction of energy lost by the gamma rays generated in the various inelastic and non-elastic reactions.

PoS(FNDA2006)012

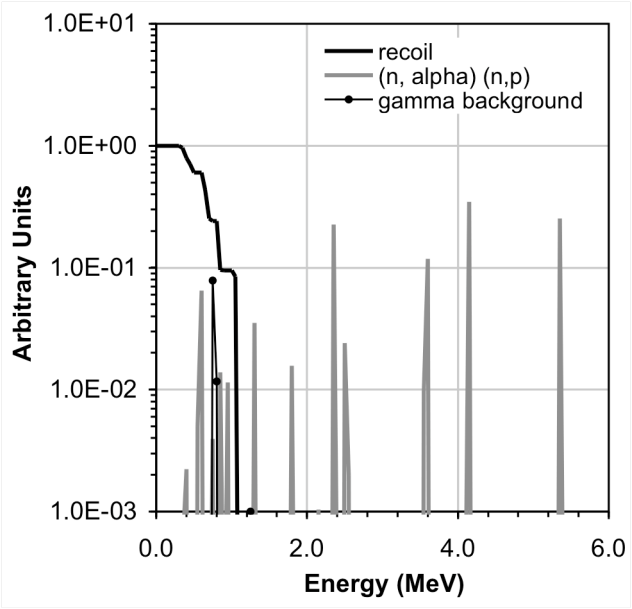

Figure 6. The components of the response function shown in Figure 5 are combined. The weighting factors from the cross section data for elastic, inelastic and non-elastic processes are taken into account. The additional weighting factors from the modelling of the interaction of gamma rays with the absorber are also considered.

6 Phonon Generation and Propagation in Silicon

The charged particles (α-particles and protons) created by the nuclear process described above will deposit almost 100% of their energy via ionisation along the particle track. Assuming an 8 MeV initial neutron, the resulting 4.14 MeV protons have a range of ~ 158 μm in Si and 5.36 MeV α-particles have a range of ~ 27 μm in Si, both with increasing dE/dx along the track. As shown in Section 5 the maximum energy lost to a recoiling Si due to scattering of an 8 MeV neutron will vary uniformly from zero, to a maximum of 1 MeV. SRIM [22] calculations show that a 1 MeV Si recoil nuclei will travel ~ 1 μm in Si and lose ~ 88% of its energy via ionisation and ~ 11% direct to phonons. Lower energy recoil events will lose more energy direct to phonons with a 10 keV event having a range of ~ 180 Å loosing ~ 43% of its energy via ionisation and ~ 52% via phonons. Ionisation due to Si recoils, α-particles or neutrons will create excited electrons and holes along the particle track; these will decay by phonon emission and usually recombine at the crystal surface where there are numerous deformations and impurities. Thus the deposited energy will all ultimately end up as phonons – those phonons that propagate into the microcalorimeter make up the detected signal. One possible problem with crystalline absorbers is that 100% electron-hole recombination may not occur. Some of the deposited energy may become trapped in impurities or long lifetime electron-hole pairs. Such metastable states thus result in incomplete absorber thermalisation over short time scales and can degrade the detector resolution [23]. Frank et al. [13] present strong evidence that this is not

PoS(FNDA2006)012

the case for a high purity Si absorber but point to the work of Seidel et al. [24], where resolution loss does occur in low purity sapphire as a result of the trap states.

In any solid, phonons will scatter by anharmonic processes (inelastic phonon-phonon collisions), as well as elastic scattering off defects and isotopic impurities [25]. There are two types of 3-phonon anharmonic scattering, Normal (N) and Umklapp (U) [26] – only U scattering is responsible for providing thermal resistance, whilst the N scattering causes frequency conversion and mode (polarisation) conversion of the phonon distribution. At these low temperatures the population of high-energy phonons able to participate in U scattering rapidly decays (~ $\exp(-\Theta/2T)$ [27], where Θ is the Debye temperature and is 645 K for Si and T is the operating temperature; hence phonon-phonon collisions become ineffective in providing thermal resistance. In this regime λ (the phonon mean free path) becomes very large (~ cm) and can exceed the specimen size, therefore the phonon mean free path is limited by the dimensions of the absorber and the quality of the crystal and crystal surfaces. If the crystal is of high purity and surface scattering is specular, then ballistic phonon transport of low energy phonons can occur. Diffuse scattering of phonons by impurities and surface roughness can reduce the thermal conductivity [28]. If diffuse surface scattering occurs then the mean free path will equal the smallest dimension of the absorber $\lambda = d$ (the absorber thickness).

Particle interactions in the absorber will create an excited distribution of phonons with average energy corresponding, approximately, to the Debye energy (~ 60 meV for Si) with a characteristic Debye frequency of ν_D ~ 13 THz. These phonons will be subject to spontaneous decay via anharmonic processes and have life times of 10-100 ps [25], thus their mean free path is very small (100 nm) compared to the specimen size. The average lifetime of the phonons becomes longer as the phonons down convert since the anharmonic decay rate, τ_A^{-1}, rapidly slows with decreasing frequency ν. Averaged over all modes the anharmonic decay rate is [25]:

$$\tau_A^{-1} = A\nu^5, \tag{5}$$

where $A = 1.2\times10^{-55}$ s^3 [38]. Silicon does not exist in a single isotope thus phonons will also scatter off isotopic impurities at a rate τ_I^{-1} (in the low frequency limit $\nu << \nu_D$) given by [25]:

$$\tau_I^{-1} = B\nu^4, \tag{6}$$

where $B = 2.43\times10^{-42}$ s^3 [38]. Assuming the surface reflection is specular, ballistic transport will occur as λ_A becomes larger than the crystal dimensions. Quasi-diffuse [25, 29-32] transport can arise, in which both ballistic and diffuse components exist, if the elastic isotopic impurity scattering rate is comparable to the anharmonic one $\tau_I^{-1} \sim \tau_A^{-1}$ (with both process occurring several times over an experimental time scale). This process has been extensively investigated in Si with ballistic contributions experimentally observed in α-particle, X-ray and neutron experiments [35]. For example, observations of ballistic phonon transport in a Si absorber with

PoS(FNDA2006)012

a Ti TES [33, 34] due to α-particle interactions, show ~ 1/3 of the transported phonons in a 1 mm crystal were found to traverse the crystal ballistically. A quasi-diffusive state can have the adverse effect of spreading the phonon arrival time thus blurring the prompt signal detected in the microcalorimeter [36]. Phonon propagation is further complicated by the dependence upon the crystallographic orientation of the specimen. The ballistic energy flow can be enhanced in some directions and suppressed in others due to phonon focusing [37] resulting from elastic anisotropy of the crystal lattice and the thermal conductance has thus been shown to depend on the orientation of the absorber axis [38]. For Si it is shown that transverse phonons are most strongly focused in the [100] direction. The work by Peterreins et al. [39], using superconducting tunnel diodes on a Si wafer absorber demonstrate the possibility of using phonon focusing patterns to obtain spatial resolution. If we consider an event at one end of the DROID (with a L = 10 cm long absorber); for a phonon to arrive ballistically at the other TES it must travel L = 10 cm without scattering. Thus setting the scattering time to the ballistic transit time: L/v_s ~ 17 μs, where v_s is the Debye speed of sound or 5990 m/s in Si, the phonon frequency for ballistic transport is then ~ 0.87 THz. Thus we calculate that a 0.87 THz phonon will have an isotopic scattering time constant of τ_I = 0.73 μs (λ_I ~ 4.3 mm, comparable to the width of the absorber). In this situation $\tau_A >> \tau_I \sim d$, and the thermal transport should be diffuse. If the surface scattering is also assumed to be diffuse then the associated boundary scattering time constant will be ~ 0.91 μs (d/v_s) and will further restrict the ballistic transport. We therefore estimate that the dominant diffusive phonon transport process should not contribute to a significant degradation of the intrinsic detector resolution. This estimate is based on the concept of a 10 cm long absorber with a TES at each end. Experimental verification is required to determine if this phonon model applies in this case.

7 Conclusion

In this study we present the concept and response function for a cryogenically cooled fast neutron spectrometer consisting of a silicon absorber and transition edge sensors. The fundamental aim of this study is therefore to understand the feasibility of developing a detector sensitive to fast neutrons above 5 MeV for spectroscopic applications. In the paper we address the need for high resolution fast neutron spectroscopy detectors that will go beyond the time of flight techniques currently available. In this paper we have described the thermodynamic rational behind our absorber and TES geometry. The study summarises the interaction processes involved when fast neutrons interact with Si, of particular interest are the non-elastic reactions generating charged particles such as protons and alphas, which have a particular energy signature; however the MCNPXTM modelling indicates that the interaction of neutrons with the detector will be dominated by elastic scattering.

The modelled response function shows that the dominant feature is the recoil distribution from elastic scattering. Non-elastic scattering will generate a number of alpha and proton peaks

PoS(FNDA2006)012

depending on the excited state reached by the compound nucleus; however, the primary alpha and proton peaks at 5.4 MeV and 4.1 MeV produced by 8 MeV neutrons in Si are clearly resolvable from the lower energy peaks given an intrinsic resolution of the order of 10 keV. The gamma rays generated by inelastic and non-elastic processes will have energies exceeding 1 MeV and will deposit small amounts of energy in the absorber. Only gamma rays travelling along the 10 cm length of the absorber will contribute the most to the gamma ray background.

The resolution of the system will not be limited by the detector but by the energy distribution of the neutron source. The limitation in detector time resolution to ~10 ms implies that it would lend itself to neutron counting applications where fluxes are low or that the flux would have to be reduced in order to allow the detector to cope. Improvements in the signal processing electronics may improve the time resolution. This type of detector may therefore be better suited to space applications, where neutron fluxes of the order of a <10 counts cm-2 s-1 [40] and one would not expect more that ~10 detected counts in the 10 cm long absorber per second; spectra could therefore be acquired over very long periods of time, given no timing resolution constraints.

The phonon generation process in the absorber and the limitations placed on the spatial resolution are also discussed. We have estimated that the dominant diffusive phonon transport process should not contribute to a significant degradation of the intrinsic detector resolution. This estimate is based on the concept of a 10 cm long absorber with a TES at each end. Experimental verification is required to determine if this phonon model applies in this case.

We have shown that the use of a Si absorber and transition edge sensor for neutron spectroscopy is feasible from a theoretical perspective; our aim is to incorporate these ideas in an experimental programme.

PoS(FNDA2006)012

References

[1] J. I. W. Watterson, R. M. Ambrosi, Nucl. Instr. and Meth. A 513 (2003) 367.
[2] C. Gongyin, R. C. Lanza, IEEE Transactions on Nuclear Science 49 (2002) 1919.
[3] R. M Ambrosi, J. I. W. Watterson, Nucl. Instr. and Meth. B 139 (1998) 279.
[4] J. Guzek, K. Richardson, C. B. Franklyn, et al., Nucl. Instr. and Meth. B 152 (1999) 515.
[5] I. Mitrofanov, D. Anfimov, A. Kozyrev, Science 297 (2002) 78.
[6] J. Guzek, PhD Thesis, Elemental Radiography Using Fast Neutron Beams, University of the Witwatersrand (1999).
[7] http://www.nucastrodata.org
[8] K. D. Irwin, App. Phys. Letts. 66 (1995) 1998.
[9] A. Fleischmann, M. Link, T. Daniyaro, H. Rotzinger, C. Enss, G. M. Seidel, Nucl. Instr. and Meth. A 520 (2004) 27.
[10] A. N. Parmar, M. Arnaud, X. Barcons, J. Bleeker, G. Hasunger, H. Inoue, G. Palumbo, M. Turner, SPIE, 5488 (2004) 388.
[11] P. de Marcillac, N. Coron, J. Leblanc, et al., Nucl. Instr. and Meth. A 337 (1993) 95.
[12] C. S. Silver, J. Beeman, L. Picirillo, et al., Nucl. Instr. and Meth. A 485 (2002) 615.

[13] M. Frank, D. Dummer, S. Cooper, et al., Nucl. Instr. and Meth. A 345 (1994) 367.
[14] T. Niedermayr, I. D. Hau, T. Miyazaki, et al., Nucl. Instr. and Meth. A 520 (2004) 70.
[15] E. Figueroa-Feliciano, Nucl. Instr. and Meth. A 520 (2004) 496.
[16] S. J. Smith, C. Whitford, G. W. Fraser, et al., Nucl. Instr. and Meth. A 520 (2004) 449.
[17] S. J. Smith, C. H. Whitford, G. W. Fraser, D. J. Goldie, Characterisation and Modelling of Transition Edge Sensor Distributed Read-Out Imaging Devices, In press Nucl. Instr. and Meth. A.
[18] S. J. Smith, Development of Transition Edge Sensor Distributed Readout Imaging Device for X-ray Astronomy Applications, PhD Thesis, PhD Thesis, University of Leicester, submitted May 2006.
[19] S. J. Smith, C. H. Whitford, G. W. Fraser, Nucl. Instr. and Meth. A 556 (2006) 237..
[20] L. S. Waters, Monte Carlo N-Particle Transport Code - X (MCNPX), Version 2.5e (2004).
[21] K. S. Krane, Introductory Nuclear Physics, Wiley, 1988.
[22] J. F. Ziegler, Stopping and Range of Ions in Matter (SRIM), www.srim.org.
[23] D. McCammon, M. Juda, J. Zhang, et al., IEEE Transactions on Nuclear Science 33 (1986) 236.
[24] W. Seidel, G. Forster, W. Christen, et al., Phys. Letts. B 236 (1990) 483.
[25] H. J. Maris, Phys. Rev. B 41 (1990) 9736.
[26] C. Kittel, Introduction to Solid State Physics (6th ed), 1995.
[27] J. R. Hook, H. E. Hall, Solid State Physics (2nd ed.), John Wiley and Sons (1999).
[28] H. B. G. Casimir, Physica V 6 (1938) 495.
[29] S. E. Esipov, Phys. Rev. B 49 (1994) 716.
[30] S. Tamura, Journal of Low Temperature Physics 93 (1993) 433.
[31] W. E. Bron, Y. B. Levison, J. M. O'Connor, Phys. Rev. Letts. 49 (1982) 209.
[32] T. E. Wilson, F. M. Lurie, W. E. Bron, Phys. Rev. B 30 (1984) 6103.
[33] B. A. Young, B. Cabrera, A. T. Lee, Phys. Rev. Letts. 64 (1990) 2795.
[34] B. A. Young, B. Cabrera, A. T. Lee, et al., Nucl. Instr. and Meth. A 311 (1992) 195.
[35] B. Cabrera, P. L. Brink, S. W. Leman, et al., Nucl. Instr. and Meth. A 520 (2004) 502.
[36] R. Horn, J. P. Harrison, Journal of Low Temperature Physics 133 (2003) 291.
[37] B. Taylor, H. J. Maris, C. Elbaum, Phys. Rev. Letts. 23 (1969) 416.
[38] A. K. McCurdy, H. K. Maris, C. Elbaum, Phys Rev. B 2 (1970) 4077.
[39] Th. Peterreins, F. Probst, F. von Feilitzsch, et al., Phys. Letts. B 202 (1988) 161.
[40] R. C. Reedy, W. C. Feldman, B. L. Barraclough, 61st Annual Meteoritical Society Meeting (1998).

PoS(FNDA2006)012